To appear in Journal of the Mechanics and Physics of Solids

A METHODOLOGY TO ASSESS THE RATE AND PRESSURE SENSITIVITY OF POLYMERS OVER A WIDE RANGE OF STRAIN RATES

D. Rittel (*) and A. Dorogoy

Faculty of Mechanical Engineering, Technion – Israel Institute of Technology

32000 , Haifa, Israel

ABSTRACT

This paper details a methodology to test the mechanical response of soft, pressure sensitive materials, over a wide range of strain rates. A hybrid experimental-numerical procedure is used to assess the constitutive parameters. The experimental phase involves axial compression of a cylindrical specimen which is confined by a tightly-fit sleeve that is allowed to yield plastically, thus applying a constant confining pressure. The usually neglected frictional effects between the specimen and the sleeve are fully accounted for and characterized in detail. With commercial polycarbonate as a typical example, it is shown that pressure-sensitivity and rate-sensitivity are not coupled, thus reducing the number of tests needed to characterize a material. The results of numerical simulations indicate that the pressure sensitivity index (angle β in the Drucker-Prager material model) has little influence on the hydrostatic and confining pressures, whereas the equivalent stress sustained by the specimen increases with β, which for commercial polycarbonate is found to be $\beta = 15^0$.

Keywords: polycarbonate, Drucker-Prager, confinement, friction, strain-rate

(*) Corresponding author: merittel@technion.ac.il

Introduction

Polymers possess excellent mechanical and machining properties that make them attractive candidates for selected structural applications, including high strain-rate impacts as encountered in aeronautical and automotive cases. The elastic–plastic behavior of polymers is markedly different from that of metals, as dictated by the pressure-dependence of their yield criterion.

The quasi-static and viscoelastic properties of polymers are well documented, for instance in the books of Christensen (1982), and Ward (1983). The high strain-rate response of these materials has been studied to a lesser extent, mostly based on split-Hopkinson (Kolsky, 1949) pressure bar experiments over a variety of strain rates (Arruda, et al., 1995; Li and Lambros, 2001; Rittel, 1999; Trojanowski, et al., 1997). The thermomechanical aspects of the high-rate response of polymers have been addressed by a few authors who studied the evolution of the temperature during impact tests (Rittel, 1999). Yet, all these references concern the behavior of unconfined polymers so that the pressure effects were left aside in this regime.

Various techniques have been developed to study confined materials, starting with Bridgman (1945), and nowadays a routinely used technique consists of enclosing the (cylindrical) specimen into a tightly fit metallic sleeve. The sleeve can either remain elastic, or yield depending on the nature of the required confinement (variable or constant). Ma and Ravi-Chandar (2000) used confined cylinders and thick elastic sleeves to study the quasi-static response of commercial polycarbonate (see also Bardia and Narasimhan (2006)). Chen and Ravichandran (1997), (2000), (1996), investigated the dynamic response of confined ceramics, while Lu and Ravichandran (2003) investigated bulk metallic glasses in the quasi-static and dynamic regime. In these tests, strain gauges were cemented to the confining sleeve to characterize the stress state of the specimen. More recently, Hanina et al. (2007) applied a plastically yielding sleeve technique to confined metallic specimens in order to study the adiabatic shear banding response to hydrostatic pressure. These authors proposed a simple superposition procedure to assess the stress state of the specimen. The same technique was applied by Rittel and Brill (2008) to investigate the quasi-static and dynamic response of commercial polymethylmethacrylate. Here, the confining pressure had to be determined analytically in a separate calculation due to the pressure sensitivity of the investigated material. These authors reported a brittle to ductile transition in this polymer, as a

function of the strain rate and level of confinement. Polymethylmethacrylate was modeled as a rate-sensitive Drucker-Prager material for which a simple constitutive equation was proposed. This work suggested that if one can show that the pressure sensitivity of the material is not rate-dependent, one can study *separately* the pressure-sensitivity and the rate sensitivity, which are ultimately combined into a single constitutive equation. However, all the above-mentioned studies have one common assumption, namely that the frictional stresses, especially at the specimen-sleeve interface, are negligible, and this assumption has not been experimentally supported so far (see e.g. Chocron et al. (2008)). However, a few recent papers, such as that of Forquin et al. (2008) did take friction into account to analyze the behavior of confined concrete.

Therefore, the main objective of this work was to develop and validate a general methodology to investigate the pressure and rate sensitivity of polymers without neglecting frictional stresses. This study focuses on commercial polycarbonate, as a typical soft and ductile polymer, which is also assumed to obey the Drucker-Prager yield function. In comparison to previous works this investigation uses several combinations of sleeve thickness and materials, allowing for constant confinement levels of up to 360 MPa, which are significantly larger than the yield strength of this material (about 5 times). Such high constant confinement levels were not attained in previous studies of that type. The approach is of a hybrid experimental-numerical nature, in which the behavior of the sleeve and the frictional effects are modeled numerically, based on measured load-displacement curves.

The main point of this paper concerns the lack of coupling between rate and pressure sensitivity for soft materials that leads to a methodology to investigate the mechanical response of soft confined pressure sensitive materials.

The paper is therefore divided into two main sections. The first section describes the experimental procedure and results, while the second section describes the verification and validation of the numerical procedures used in this study. These two main sections are followed by a discussion section and concluding remarks.

2. Experimental methods and specimens

Cylindrical specimens (6mm diameter and height), confined and unconfined, were subjected to quasi-static and dynamic compression tests. The quasi-static

experiments were performed on an MTS 810 servo-hydraulic machine under displacement control at various strain rates. The dynamic (high strain rate) experiments were performed on a 12.7 mm diameter split Hopkinson (Kolsky) pressure bar. The specimens were confined by manual insertion of the lubricated specimen into tightly machined metallic sleeves, made of different materials and wall thickness, as detailed for each test. The choice of different sleeve materials and thicknesses was motivated by the need to achieve a wide range of confining pressures, as detailed in the sequel. The specimen assembly is seen in Fig. 1. Each specimen is made of three parts: a cylindrical polycarbonate specimen, a metal sleeve and an adapter. These parts are seen in Fig. 1(a-c), respectively. The polycarbonate cylindrical specimen (Fig. 1(a)) is tightly fit into the sleeve (Fig. 1(b) and 1(d)), which is half a millimeter longer than the specimen. The cylindrical adapter (Fig. 1(c)) is put on top of the confined specimen, thus completing the assembly (Fig. 1(e)). The loaded specimen is shown in Fig. 1(f). When a split Hopkinson pressure bar is used, the adapter is always located towards the incident bar to transmit the impact.

Data reduction consisted of translating the load-displacement records into true stress-strain curves. For the unconfined specimens, this is a straightforward procedure, based on the simplifying assumption of plastic incompressibility. Previous work on confined specimens has shown that the confining pressure can be determined from the flow properties of the sleeve at the appropriate strain-rate, based on the elastic-plastic analysis of a thick-walled cylinder in a direct manner (Rittel and Brill, 2008). This approach is based on the assumption of a negligible friction between the specimen and the sleeve. The present work re-examines the validity of this assumption, and shows that the accuracy of the results is improved when frictional stresses are included. A detailed account of the analytical-numerical procedure that was developed to account for friction is presented in detail subsequently.

3. Approximate determination of the Drucker Prager pressure sensitivity index

The Drucker Prager plasticity model is given by (Bardia and Narasimhan, 2006)

$$\Phi\left(\sigma_{ij},\sigma_c\right)=\sigma_{eq}+p\tan\beta-\left(1-\frac{1}{3}\tan\beta\right)\sigma_c=0 \qquad (1)$$

Where $\sigma_c\left(\varepsilon_p, \dot{\varepsilon}\right)$ is the true yield stress under uniaxial compression which is a function of the equivalent plastic strain and strain rate. The pressure sensitivity index, is noted by β, and σ_{eq} is the Mises equivalent stress. It can be noted that for $\beta = 0$ Eqn. (1) reduces to the Von Mises yield function. The Mises equivalent stress is given by:

$$\sigma_{eq} = \sqrt{3\,\mathrm{J}_2} = \sqrt{\frac{3}{2} s_{\mathrm{ij}} s_{\mathrm{ij}}} \tag{2}$$

where s_{ij} is the deviatoric stress:

$$s_{ij} = \sigma_{ij} - \delta_{ij} p \tag{3}$$

and where p is the hydrostatic stress:

$$p = \frac{\sigma_{ii}}{3} \ . \tag{4}$$

The confining pressure exerted by the elastic-plastic sleeve can be calculated analytically (Kachanov, 1974). Rittel and Brill (2008) calculated an average confining pressure $\hat{\mathrm{q}}$ for an elastic plastic cylindrical sleeve with inner radius *a*, thickness *t* and yield stress σ_{y}:

$$\hat{q} = \frac{1}{2}\left(q_{r=a} + q_{r=a+t}\right) = \frac{\sigma_Y}{4}\left(1 - \left(1 + \frac{t}{a}\right)^{-2} + 2\ln\left(1 + \frac{t}{a}\right)\right) \tag{5}$$

It should be noted that this average value is indirectly taking frictional effects into account which lowers the confining pressure as will be shown in the sequel. Assuming Coloumb friction (with a coefficient of friction *f*) between the polycarbonate cylinder and the confining sleeve introduces a shear stress on the outer face of the cylinder σ_{rz}, according to Fig. 2.

$$\sigma_{\mathrm{rz}} = -f\,q \tag{6}$$

Where $q \equiv \sigma_{rr}\left(r = a\right)$. The stress tensor in the cylinder may be approximated by:

$$\sigma_{ij} = \begin{bmatrix} q & 0 & -f\,q \\ 0 & q & 0 \\ -f\,q & 0 & \sigma_{zz} \end{bmatrix} \qquad i, j = r, \theta, z \tag{7}$$

The hydrostatic pressure is given by

$$p = \frac{1}{3}\left(\sigma_{zz} + 2q\right) \tag{8}$$

From Eqs. (2) and (7), the equivalent stress becomes:

$$\sigma_{eq} = \sqrt{(\sigma_{zz} - q)^2 + 3(f\,q)^2} \tag{9}$$

Throughout this work, it was assumed that $f = 0.3$, in accord with Lee *et al.* (2001), without differentiating between static and dynamic friction. It was also assumed that $q = -\hat{q}$. For different experiments carried out at approximately the same strain rate, a plot of the equivalent stress (Eqn. (9)) vs. the hydrostatic pressure (Eqn. (8)) should result in a straight line with a slope angle β which is the pressure sensitivity index (Eqn. (1)).

4. Experimental results

4.1 The sleeves' mechanical properties

Four different materials were used as sleeves: maraging steel 250 (H900), and 300 (H900), 1020 steel (as-received), and 6061 T651 aluminum alloy. The mechanical properties of these materials are listed in table 1. These properties were either measured quasi-statically and dynamically, using small cylindrical specimens, or simply taken from the literature (Brill, 2007; Dao, et al., 2001; Regev and Rittel, 2008), as detailed in table 1.

4.2 Polycarbonate: Quasi-static tests

A total of 13 specimens were tested. The thickness of the sleeves, their material and the strain rates of the experiments are listed in table 2.

Three specimens were not confined (specimens 1-3), four were confined with sleeves made of 250 maraging steel (specimens 4-7), and six were confined with 300 maraging steel (specimens 8-13).

The true stress–strain curves of the non confined specimens (1-3) are shown in Fig 3. Two more curves which were obtained at strain rates of 4900 1/s (this work) and 8000 1/s (Regev and Rittel, 2008) are added to this figure to illustrate the well-known strain-rate sensitivity of commercial polycarbonate.

Typical true stress-strain curves of confined specimens are shown in Fig. 4(a) (specimens 4-7), and 4(b) (specimens 8-13). The pressure sensitivity of the

polycarbonate specimens is clearly observed in Fig. 4: the thicker the sleeve the higher the max stress. This corresponds to the fact that thicker sleeves apply higher confinement pressures which delay the yield of the polycarbonate specimen.

4.3 Polycarbonate: Dynamic tests

A total of 24 (7 unconfined, 17 confined) specimens were tested dynamically. The sleeves' thickness, material and strain rate of the experiments are detailed in table 3. Typical striker velocities ranged between 20-35 m/s , resulting in average strain rates of 3600 – 5600 1/s. Typical dynamic experimental results are shown in Fig. 5. The peak stresses on Fig. 5(a) which correspond to the three types of sleeves (0.5 mm-250 maraging steel, 0.3 mm-250 maraging steel, and 0.7 mm 6061 aluminum) are: ~450 MPa , ~330 MPa and ~200 MPa correspondingly. The effect of the confinement pressure on the peak stress is clearly visible. The higher the confinement stress, the higher the peak stress. The same effect is also visible in Fig. 5(b) for different thicknesses of 1020 steel sleeves . The overall pressure sensitivity of the polycarbonate specimens is clearly observed in quasi static experiments (Fig. 4) as well as in dynamic experiments (Fig. 5)

4.4 Processed experimental results

The experimental peak stresses σ_{zz} are detailed in tables 2-3 for each specimen. For the specimens with steel sleeves, the peak stress σ_{zz} at 11 % was used (assuming the sleeve broke at this strain). The calculated values : $\hat{q}$, p and σ_{eq} according to eqs. (5), (8) and (9) for quasi static and dynamic tests are tabulated in tables 2 and 3 respectively.

The equivalent stresses and pressures of tables 2 and 3 are plotted in Fig. 6, in order to determine the Drucker-Prager pressure sensitivity index β of Eqn. (1). Using a linear regression, the angle β for the quasi static loading is $\beta_{qs} = 19.6^0$ with R^2 = 0.95 (13 specimens). The angle β for the dynamic loading is $\beta_d = 15.1^\circ$ with R^2 = 0.89 (24 specimens). Two almost parallel lines (within the expected error limits detailed in the next section) are shown in Fig. 6, where the dynamic curve is above the quasi-static, illustrating the strain rate sensitivity of the polycarbonate.

4.5 Error estimation

Let's assume we conducted only two experiments so that only have two points (1) and (2), on a σ_{eq}-p curve, such as Fig. 6. The values of the pressure and the equivalent stress at these points are given by Eqns. (8) and (9). Let us also assume that point (1) corresponds to a unconfined specimen thus $q^{(1)} = 0$. The expression for the angle β is

$$\beta = \tan^{-1}\left[3\frac{\sigma_{zz}^{(1)} - \sqrt{\left(\sigma_{zz}^{(2)} - q^{(2)}\right)^2 + 3\left(fq^{(2)}\right)^2}}{\sigma_{zz}^{(1)} - \sigma_{zz}^{(2)} - 2q^{(2)}} \right] \tag{10}$$

If we assume that the coefficient of friction f is known, the error in the angle β is given by:

$$\Delta\beta = \frac{\partial\beta}{\partial\sigma_{zz}^{(1)}}\Delta\sigma_{zz}^{(1)} + \frac{\partial\beta}{\partial\sigma_{zz}^{(2)}}\Delta\sigma_{zz}^{(2)} + \frac{\partial\beta}{\partial q^{(2)}}\Delta q^{(2)} \tag{11}$$

Let us assume that points (1) and (2) correspond to specimens 1 and 13 of table 2. Let us assume that the values $\sigma_{zz}^{(1)} = 70$ MPa, $\sigma_{zz}^{(2)} = 413$ MPa and $q^{(2)} = 323$ MPa have a 10% error, so that $\Delta\sigma_{zz}^{(1)} = \pm 7$ MPa, $\Delta\sigma_{zz}^{(2)} = \pm 41$ MPa and $\Delta q^{(2)} = \pm 32$ MPa. Plugging these (absolute) values into Eqns. (11) and (10) leads to: $\Delta\beta^\circ = 0.9^\circ + 2.2^\circ + 1.7^\circ = \pm 4.6^\circ$. Assuming lower values of *f*, Eq. 10 will result in lower values of β. For example for f = 0, 0.15 and 0.30, Eq. 1- results in β = 3.5° , 9.1° and 20.1° respectively. However, the real error bounds might even be larger, since by assuming a stress tensor of the type shown in Eqn. (5), the confinement pressure q and the shear stress due to friction are deemed to be uniform through the whole cylindrical specimen which is of course an approximation. This assumption is discussed later at in the "numerical results" section, where the final value of β is determined.

4.6 Strain rate effect on $\sigma_c\left(\varepsilon_p\right)$ - unconfined specimens

The peak stresses of the unconfined experiments (Fig. 3) versus their corresponding strain rates are plotted in Fig. 7. It is assumed that the peak stress occurs at approximately the same plastic strain for each test. The data is fitted by a power law: $\sigma_c^{peak} \cong 89.8\ \dot{\varepsilon}^{\,0.03871}$ [MPa] as shown in Fig. 7. This result illustrates the fact that, since the pressure sensitivity is not rate-dependent, pressure and rate sensitivity of the

material can be addressed separately and combined into a simple constitutive equation. It should be noted that the proposed power law is of the simplest phenomenological nature, while more sophisticated constitutive models have been proposed for polymers, see e.g. Mulliken and Boyce (2006), or Richeton et al. (2005).
The next part of the paper addresses numerical simulations that are used to validate the overall data-reduction technique presented in the experimental section.

5. Numerical verification and validation

Quasi-static and transient simulations were performed for two reasons. The first is to verify the values of the pressure sensitivity index β which was approximately determined experimentally. β was chosen by a trial and error procedure until a satisfactory agreement between all experimental results and numerical simulations was achieved. A second reason is the characterization of the stress and strain distribution in the polycarbonate cylinder under the effect of friction together with the dissipated frictional energy.

We first introduce the various parameters of the numerical simulations. Next comes the validation of the quasi-static and dynamic values of β. The stress and strain distribution in the frictional polycarbonate specimen are presented next, followed by an assessment of the amount of dissipated frictional energy. This study also includes the effect of β on the average values of the p, q and σ_{eq}.

5.1 Parameters of the numerical simulations

5.1.1 Analyses type

Numerical simulations were performed with the commercial finite element code Abaqus explicit version 6.7. The analyses were transient and the model was axisymmetric. The typical duration of the experiment was set to 120 μs for dynamic tests and to 0.01 s for quasi-static tests. The assembly is shown in Fig. 8(a). A typical meshed model is shown in Fig. 8(b).

5.1.2 Mesh properties

The model was meshed with CAX4R elements. This element is a 4-node bilinear axisymmetric quadrilateral element with reduced integration and hourglass control. A typical mesh, like the one shown in Fig. 8(b), is comprised of 5322 elements of average size of 0.125 mm where 1600 elements have been generated for the adapter, 3200 elements for cylindrical specimen and 522 for the sleeve.

5.1.3 Material properties

Elastic-plastic material models were assigned to the adapter and the sleeves, whose quasi-static and dynamic mechanical properties were measured (see also table 1).
The polycarbonate specimen was assumed to obey the Drucker-Prager material model, with properties listed in table 4. Experimentally determined stress-strain curves for unconfined specimens at different strain rates ($\dot{\varepsilon} = 0.0005, 0.05,$ 4900 and 8000 1/s Regev and Rittel (2008)), were input for the analyses.
As a first guess we used the values obtained by the approximate determinations, namely $\beta = 15°$ (Fig. 6).

5.1.4 Boundary conditions

Radial symmetry was applied along the centerline (r = 0). Tangential contact with Coloumb friction ($f = 0.3$) was assumed between the specimen and the sleeve, as well as between the specimen and the steel adapter and also the sleeve and the adapter. In transient analyses, the measured velocities were applied to the bottom and top surfaces (Fig. 8). For quasi-static analyses, the bottom face of the specimen and sleeve were constrained from moving in the vertical z direction while a vertical velocity of 0.12 m/s for a duration of t = 0.01 s was applied to the upper face.

5.2 Validation of quasi-static experimental results

A quasi static simulation of all the specimens was performed. The averaged true stress (σ_{zz}) and true strain (ε_{zz}) along the mid-height line (Fig. 8(a)) was calculated at each time step. It was verified that these values represent an average stress-strain for the

whole cylinder. These values are then compared to the experimentally measured values. A very good agreement was reached when a value of $\beta = 15°$ was used for the polycarbonate pressure sensitivity index. A numerical-experimental comparison for specimens 10 and 12 (table 2) is shown in Fig. 9.

5.3 *Validation of the dynamic experimental results*

The validation of two cases of low (0.7 mm-6061 Al sleeve) and high (0.5 mm-250 maraging steel sleeve) confinement pressures is demonstrated in Figs. 10(a) and 10(b) respectively. These two cases correspond to specimens 5 and 9 of table 3.

The measured velocities were digitized and applied as boundary conditions for these analyses. These velocity profiles are shown in Figs. 10(c) and 10(d). These specimens were simulated using $\beta = 5^{\circ}, 10^{\circ}, 15^{\circ}$ and 20°. The averaged true stress (σ_{zz}) and true strain (ε_{zz}) at mid-height line were calculated at each time step. These values are plotted in Figs. 11(a) and 11(b) together with the experimental results. A very good agreement was reached when the value of $\beta = 15^{\circ}$ (together with the assumption of $f = 0.3$) was used for the pressure sensitivity index.

This value can be compared to previously reported results based on different experimental techniques. Quinson et al. (1997) used tension, torsion, and compression tests to determine a value of $\beta = 11.3^{\circ}$, based on Tresca's yield criterion. Ragahva et al. (1973) used pressurized tubular specimens and measured a value of $\beta = 15.3^{o}$. Carapellucci and Yee (1986) also used pressurized tubular specimens and measured a value of $\beta = 13.7^{o}$. Finally Haufe et al. (2005), using tension and compression tests, obtained a value of $\beta = 15^{\circ}$. Overall, there is an excellent agreement between the current results and those obtained using different methodologies which do not involve frictional issues, which validates the presented methodology. One should also note that the dynamic value of β is identical to that of the quasi-static tests, showing that this parameter is not rate-sensitive for this material.

5.4 Stress and strain distribution under the effect of friction

Contour maps of ε_{zz}, σ_{zz}, σ_{rr} and σ_{rz} at the high average true strain of 0.2 are plotted in Fig. 11. These maps correspond to specimens (4-6 of table 3) confined with sleeves made of 250 maraging steel which exert the maximum confinement pressure. Hence, these maps correspond to the "worst case" of inhomogeneity of the stresses and strains inside the polycarbonate cylinders. For lower values of confinement and applied strain the stresses and strain within the polycarbonate cylinder are much more homogeneous. The longitudinal strain ε_{zz} varies between $0.1 < |\varepsilon_{zz}| < 0.35$ (Fig. 11(a)). It reaches a maximum of 0.35 at the center on the bottom face and a minimum of 0.1 at the center close to the upper face. Most of the polycarbonate cylinder experiences a strain $0.125 < |\varepsilon_{zz}| < 0.3$.

The contour map of the longitudinal stress σ_{zz} is shown in Fig. 11(b). Most of the cylinder experiences a compression stress $400 \le |\sigma_{zz}| \le 600$ $[MPa]$. The higher compression stress is toward the upper face while the lower pressure stress is toward the bottom face. A stress concentration on the upper face where the edge of the adapter contacts the specimen can be observed.

The averaged values along the mid-height line (Fig. 8(a)) are those which were used for validation through comparison with the measured ones. The maps 11(a) and 11(b) show that, even for the "worst case" (high strain and high confinement pressure), the averaged value along the mid-height line is characteristic of the average value of the field for the whole cylinder.

The contour map of the radial stress σ_{rr} is plotted in Fig. 11(c). The radial stress on the outer radius of the cylinder is the confinement pressure which is estimated by Eqn. (5). σ_{rr} is quite homogeneous along the radius but does vary along the height of the cylinder. Most of the cylinder experiences $200 \le |\sigma_{rr}| \le 380$ $[MPa]$. The higher stresses are toward the upper face while the lower stresses are toward the bottom face. Once again it can be observed that the values along the mid-height line represent an average for the whole cylinder.

Finally, the effect of friction is embodied by the shear stress σ_{rz}. Fig. 11(d) shows that this stress is far from being homogeneous inside the cylinder. It is zero on the centerline ($r = 0$) and grows toward the outer radius. It varies also along the height of the cylinder and reaches a maximum of 86 MPa at mid-height. A stress concentration near the

contact region between the adapter edge and the cylinder is also observed in this figure. On the outer radius of the cylinder this shear stress is $\sigma_{rz} = -f\sigma_{rr}\left(r=a\right) \equiv -f\,q$.

An estimation of the energy dissipated by the friction between the sleeve and the cylinder during the impact is shown in Fig. 12. Abaqus integrates the external applied work and the frictional work. These quantities are plotted in Fig. 12 as a function of $\left|\varepsilon_{zz}\right|$. The percent ratio between these quantities is plotted as well. It can be observed that during the early stage of impact loading, $0.04 < \left|\varepsilon_{zz}\right| < 0.15$, an average of 15% of the externally applied energy is wasted on friction. As the strain reaches, $\left|\varepsilon_{zz}\right| = 0.3$, this ratio reduces to 10%.

5.5 Effect of β *on averaged values of* q *,p and* σ_{eq}

The impact of specimens 4-6 of table 3 was simulated using different values of β. Four values were used: $\beta = 5^{\circ}, 10^{\circ}, 15^{\circ}$ and 20°. The averaged values of q, p and σ_{eq} along the mid-height line are plotted as a function of $\left|\varepsilon_{zz}\right|$ in Figs. 13(a-c), respectively.

The following conclusions can be deduced from the numerical simulations:

1. The angle β has a minor effect on the confinement pressure. The confinement pressure ranges between 250 to 300 MPa and is quite constant for $5^{\circ} \le \beta \le 20^{\circ}$ and $0.14 \le \varepsilon < 0.25$
2. The angle β has a minor effect on the hydrostatic pressure. The hydrostatic pressure ranges between 298 to 355 MPa for $0.14 \le \varepsilon < 0.25$ and is quite constant for $5^{\circ} \le \beta \le 20^{\circ}$
3. The equivalent stress σ_{eq} is affected by β. The higher the β the higher σ_{eq}. The average value in the range $0.14 \le \varepsilon < 0.25$ is 144, 169 196 and 223 MPa for $\beta = 5, 10, 15$ and 20 degrees respectively.

6. Discussion and Conclusions

The present work has addressed the rate and pressure sensitivity of soft matter, based on commercial polycarbonate as a representative material. The employed methodology relies on a hybrid experimental-numerical procedure. The cylindrical specimen is

enclosed in a tightly-fit sleeve that is allowed to yield plastically, thus applying a constant confining pressure to the specimen.

The methodology consist of 4 steps to identify the two material parameters of Eqn. (1), namely β and $\sigma_c\left(\varepsilon_p, \dot{\varepsilon}\right)$:

1. Testing of unconfined specimens at different strain rates for determination of $\sigma_c\left(\varepsilon_p, \dot{\varepsilon}\right)$ of Eqn. (1).

2. Testing of confined specimens quasi statically and dynamically (at approximately the same strain rate).

3. Estimating the pressure sensitivity index β without neglecting frictional effect (Eqn. (9)) as detailed in section 3.

4. Verifying and refining the obtained result of step 3 numerically using a finite element code which utilizes the Drucker Prager material model and Coloumb friction between all contacting faces. The obtained $\sigma_c\left(\varepsilon_p, \dot{\varepsilon}\right)$ serves as an input and the experimentally measured velocities are applied as boundary conditions. The pressure sensitivity index β is found by a trial and error process using the obtained result of step 3 as an initial guess. The process continues until satisfactory agreement between the numerical and experimental results is achieved.

It should be noted that this methodology is applicable to many other pressure sensitive material, whether soft (e.g. polycarbonate) or hard (e.g. polymethylmethacrylate).

A first outcome of the study, in accord with the assumption made by Rittel and Brill (2008), is that pressure and strain-rate sensitivity are two uncoupled issues. While this may appear to be straightforward, the subject remained to be verified experimentally. The result of this observation is that the number of tests is considerably reduced, and it is sufficient in principle to test a few confined specimens in the quasi-static regime (step 2).

A central issue that has been overlooked is that of the friction that inevitably develops between the specimen and the sleeve, as well as between the specimen and the adapter. Careful numerical examination of the state of stress and strain in the specimen reveals that Eqn. (5), which analytically determines the confinement pressure, overestimates the real confinement by 13% (for f = 0.3). The higher the coefficient of friction, the lower the real confinement pressure. The stress state is found to have some

inhomogeneity that evolves with the time and level of confining pressure. This lack of homogeneity is also true for the frictional shear stress which decays along the specimen radius. Hence, step 3, which assumes homogeneous mechanical fields in the specimen with a simplified frictional stress model, is a first approximation that can be verified numerically as done in step 4. In this step, the numerical simulations are driven by experimentally measured parameters, allowing for the identification of the most plausible pressure sensitivity index (β) with full account of frictional effects. The numerical results of step 4 reveal that σ_{eq} increases with β. Performing step 3 (Eqn. (9)) with the common frictionless assumption (f = 0) results in lower values of σ_{eq}, hence the determined β is a lower bound.

Finally, combining the strain-rate and pressure sensitivity results for commercial polycarbonate, one obtains a simple constitutive law:

$$\sigma_{eq} + 0.268\,p = 0.911\,\sigma_c \tag{12}$$

where $\sigma_c\left(\varepsilon_p, \dot{\varepsilon}\right)$ is detailed in Fig. 3. It should be noted here that p is considered negative for the current compression tests.

Equation (12) can be further simplified by considering a specific strain (stress) level, such as the peak stress, which was approximated by $\sigma_c^{peak} \cong 89.8\,\dot{\varepsilon}^{0.03871}\ \left[MPa\right]$, similar to Rittel and Brill (2008). Assuming that $\tau_{flow} = \dfrac{\sigma_{eq}}{2}$ and $\dot{\varepsilon} = \dfrac{\dot{\gamma}}{2}$, Eqn. (12) reduces to:

$$\tau_{flow}^{peak} = 39.7\,\dot{\gamma}^{0.03871} - 0.134\,p \qquad [MPa] \tag{13}$$

To conclude, this study has presented a systematic methodology to characterize the mechanical properties of pressure sensitive materials, with a full account of frictional stresses. The various sources of error, which relate to the homogeneity of the mechanical fields in the specimen, as well as to the very distribution of the frictional stress, have been identified. Having clarified the nature and effect of each parameter on the measured properties, the proposed methodology based on the decoupling between pressure and rate effects is rather simple and of an easy implementation.

Acknowledgement: Mr. A. Reuven and A. Amon are acknowledged for their technical assistance. The support of the Technion Fund for Future Security (PMRI grants 2009509 and 2008948) is highly appreciated.

References

Arruda, E.M., Boyce, M.C., Jayachandran, A., 1995. Effects of strain rate, temperature and thermomechanical coupling on the finite strain deformation of glassy polymers. Mechanics of Materials 19, 193-212.

Bardia, P., Narasimhan, R., 2006. Characterisation of pressure-sensitive yielding in polymers. Strain 42, 187-196.

Bridgman, P.W., 1945. Flow and Fracture. AIME Trans. 162, 569-583.

Brill, A., 2007. The influence of hydrostatic pressure on the dynamic failure of PMMA. Faculty of Mechanical Engineering. Technion, Haifa, p. 100.

Carapellucci, L., Yee, A., 1986. The biaxial deformation and yield behavior of bisphenol-a polycarbonate: Effect of anisotropy. Polym. Engng and Science 26 (13), 920-930.

Chen, W., Ravichandran, G., 1996. Static and dynamic compressive behavior of aluminum nitride under moderate confinement. J. Am. Ceram. Soc. 79 (3), 579-584.

Chen, W., Ravichandran, G., 1997. Dynamic compressive failure of glass ceramic under lateral confinement. J. Mech. Phys. Solids 45 (8), 1303-1328.

Chen, W., Ravichandran, G., 2000. Failure mode transition in ceramics under dynamic multiaxial compression Int. J. Fract. 101 (1-2), 141-159.

Chocron, S., Walker, J., Nicholls, A., Dannemann, K., Anderson, C., 2008. Analytical model of the confined compression test Used to characterize brittle materials. J. Appl. Mech. 75 (2), 021006-021001.

Christensen, R.M., 1982. Theory of Viscoelasticity: An Introduction. Academic Press, New York.

Dao, M., Chollacoop, N., Vliet, K.V., Vekatesh, T., Suresh, S., 2001. Computational modeling of the forward and reverse problems in instrumented sharp indentation. Acta Mater. 49, 3899-3918.

Forquin, P., Gary, G., Gatuingt, F., 2008. A testing technique for concrete under confinement at high rates of strain. Int. J. Impact Engng. 35, 425-446.

Hanina, E., Rittel, D., Rosenberg, Z., 2007. Pressure sensitivity of adiabatic shear banding in metals. Applied Physics Letters 90 (2), 021915.

Haufe, A., Bois, P.D., Kolling, S., Feucht, M., 2005. A semi-analytical model for polymers subjected to high strain rates. 5th European LS-Dyna users conference.

Kachanov, L.M., 1974. Foundations of the Theory of Plasticity. Mir, Moscow.

Kolsky, H., 1949. An investigation of the mechanical properties of materials at very high rates of loading. Proc. Phys. Soc. London 62-B, 676-700.

Lee, J., Xu, G., Liang, H., 2001. Experimental and numerical analysis of friction and wear behavior of polycarbonate. Wear 251, 1541–1556.

Li, Z.H., Lambros, J., 2001. Strain rate effects on the thermomechanical behavior of polymers Int. J. Solids & Structures 38 (20), 3549-3562.

Lu, J., Ravichandran, G., 2003. Pressure-dependent flow behavior of Zr41.2Ti13.8Cu12.5Ni10Be22.5 bulk metallic glass J. Mat. Res. 18 (9), 2039-2049.

Ma, Z., Ravi-Chandar, K., 2000. Confined compression: A stable homogeneous deformation for constitutive characterization. Exp. Mech. 40 (1), 38-45.

Mulliken, A., Boyce, M., 2006. Mechanics of the rate-dependent elastic-plastic deformation of glassy polymers from low to high strain rates. Int. J. Solids & Structures 43, 1331-1356.

Quinson, R., Perez, J., Rink, M., Pavan, A., 1997. Yield criteria for amorphous glassy polymers J. Matls. Sc. 32 (5), 1371-1379.

Raghava, R., Caddell, R., Yeh, G., 1973. The macroscopic yield behaviour of polymers. J. Matls. Sc. Letters 8 (2), 225-232.

Regev, A., Rittel, D., 2008. Simultaneous transient temperature sensing of impacted polymers using infrared detectors and thermocouples. Exp. Mech. in press.

Richeton, J., Ahzi, S., Daridon, L., Rémond, Y., 2005. A formulation of the cooperative model for the yield stress of amorphous polymers for a wide range of strain rates and temperatures. Polymer 46, 6035-6043.

Rittel, D., 1999. The conversion of plastic work to heat during high strain rate deformation of glassy polymers. Mechanics of Materials 31 (2), 131-139.

Rittel, D., Brill, A., 2008. Dynamic flow and failure of confined polymethylmethacrylate. J. Mech. Phys. Solids in press.

Trojanowski, A., Ruiz, C., Harding, J., 1997. Thermomechanical properties of polymers at high rates of strain. J. Physique Coll. C 3, 447-452.

Ward, I.M., 1983. Mechanical Properties of Solid Polymers. J. Wiley and Sons, New York, NY.

Captions of tables

Table 1 Mechanical and physical properties of the sleeves materials. Note that (M) indicates measured property which is otherwise taken from the literature

Table 2 Quasi-static loading: Details of the dynamic tests and calculated absolute values of $\hat{q}$ (confining pressure,) p (hydrostatic pressure) and σ_{eq} (equivalent stress)

Table 3 Dynamic loading: Details of the dynamic tests and calculated absolute values of $\hat{q}$ (confining pressure), p (hydrostatic pressure) and σ_{eq} (equivalent stress)

Table 4 Polycarbonate properties

TABLES

Table 1: Mechanical and physical properties of the sleeves materials. Note that (M) indicates measured property which is otherwise taken from the literature

property	Maraging steel 250	Maraging steel 300	Aluminum 6061 T651	Steel 1020
ρ $[Kg/m^3]$	8000	8000	2700	7800
E [GPa]	210	210	69	210
ν	0.3	0.3	0.33	0.3
σ_Y^{static} [MPa]	1790	2250 (M)	-	-
$\sigma_Y^{dynamic}$ [MPa]	2200 (M)	-	350	840 (M)

Table 2: Quasi-static loading: Details of the dynamic tests and calculated absolute values of $\hat{q}$ (confining pressure,) p (hydrostatic pressure) and σ_{eq} (equivalent stress).

specimen	t [mm]	Sleeve material	Strain rate [s^{-1}]	σ_Y [MPa] Sleeve	$\hat{q}$ $[MPa]$	σ_{zz} $[MPa]$	p $[MPa]$	σ_{eq} $[MPa]$
1	-	unconfined	$5x10^{-4}$	0	0	70	23	70
2	-	unconfined	$5x10^{-3}$	0	0	74	25	74
3	-	unconfined	$5x10^{-2}$	0	0	77	26	77
4	0.32	M 250	$5x10^{-4}$	1790	173	255	200	122
5	0.32	M 250	$5x10^{-4}$	1790	173	253	200	120
6	0.50	M 250	$5x10^{-4}$	1790	257	372	295	176
7	0.50	M 250	$5x10^{-4}$	1790	257	353	289	165
8	0.27	M 300	$5x10^{-4}$	2250	186	250	207	116
9	0.27	M 300	$5x10^{-4}$	2250	186	251	208	116
10	0.30	M 300	$5x10^{-4}$	2250	205	289	233	136
11	0.50	M 300	$5x10^{-4}$	2250	323	401	349	185
12	0.50	M 300	$5x10^{-4}$	2250	323	414	353	191
13	0.50	M 300	$5x10^{-4}$	2250	323	413	353	190

Table 3: Dynamic loading: Details of the dynamic tests and calculated absolute values of $\hat{q}$ (confining pressure), p (hydrostatic pressure) and σ_{eq} (equivalent stress) .

specimen	t [mm]	Sleeve material	Strain rate [s^{-1}]	σ_Y [MPa] Sleeve	$\hat{q}$ [MPa]	σ_{zz} [MPa]	p [MPa]	σ_{eq} [MPa]
1	0.3	M 250	3800	2200	200	309	237	150
2	0.3	M 250	3600	2200	200	330	244	166
3	0.3	M 250	3800	2200	200	316	239	156
4	0.5	M 250	3800	2200	315	450	360	212
5	0.5	M 250	3900	2200	315	452	361	213
6	0.5	M 250	4300	2200	315	460	364	219
7	0.7	Aluminum 6061	4900	350	67	213	115	150
8	0.7	Aluminum 6061	5000	350	67	207	113	145
9	0.7	Aluminum 6061	5000	350	67	210	114	147
10	0.7	Aluminum 6061	4800	350	67	205	113	143
11	0.7	Aluminum 6061	5000	350	67	202	112	140
12	0.3	Steel 1020	4400	840	76	214	122	143
13	0.3	Steel 1020	4400	840	76	218	124	150
14	0.48	Steel 1020	4100	840	116	232	155	131
15	0.48	Steel 1020	4100	840	116	240	158	138
16	0.7	Steel 1020	4400	840	160	287	202	152
17	0.7	Steel 1020	4300	840	160	291	204	155
18	-	Unconfined	4100	-	-	110	37	110
19	-	Unconfined	4900	-	-	115	38	115
20	-	Unconfined	4100	-	-	125	42	125
21	-	Unconfined	3600	-	-	120	40	120
22	-	Unconfined	4800	-	-	115	38	115
23	-	Unconfined	5600	-	-	119	40	119
24	-	Unconfined	5600	-	-	116	39	116

Table 4 : Polycarbonate properties

property	polycarbonate
ρ $[Kg/m^3]$	1200
E [GPa]	2.2
ν	0.37

Captions of figures

Fig. 1. The specimen assembly. a. Cylindrical polycarbonate specimen. b. Metallic sleeve. c. Adapter which is used to apply pressure to (a). d. Assembly of the specimen into the sleeve. e. Assembly of the adapter (c) on top of the confined specimen. f. The assembled specimen under quasi-static compression testing.

Fig. 2. A cylinder with an outer radius a and a sleeve of thickness t with cartesian and cylindrical coordinate systems attached to it.

Fig. 3. True stress–strain curves for unconfined specimens (1-3) along with typical dynamic results. The high strain-rate sensitivity of PC is noticeable.

Fig. 4. Quasi static experimental results of confined specimens. a. Specimens 4-7 of table 2 confined with sleeve made of M 250 steel . b. Specimens 8-13 of table 2 confined with sleeves made of M 300 steel.

Fig. 5. Dynamic experimental results . a. Specimens 1, 2, 5 and 6 of table 3 confined with M 250 sleeves, and specimens 7-8 of table 3 confined with aluminum 6061 sleeves. b Specimens 12-17 of table 3 confined with 1020 steel sleeves.

Fig. 6 Quasi static and dynamic experimental results of the equivalent stress vs. pressure.

Fig. 7 Strain rate sensitivity of unconfined polycarbonate. The stress is measured at its peak value.

Fig. 8 The axisymmetric assembly model with a coordinate system and arrows indicating the location of the applied velocities in the dynamic simulations. a. The geometrical model which consists of three parts: specimen, sleeve and adapter. b. A typical meshed model with quadrilateral elements.

Fig. 9 Comparison of the experimental stress-strain curve of specimens 10 and 12 of table 2 to the numerical stress strain obtained by solving quasi- statically with the assumption of $f = 0.3$ and $\beta = 15^{\circ}$. Note the very good agreement between the experiments and the simulations for this set of parameters

Fig. 10 Numerically calculated stress strain curves for $f = 0.3$ and $\beta = 5^{\circ}, 10^{\circ}, 15^{\circ}$ and 20°, and experimental results together with their corresponding typical applied velocities. The specimens are detailed in table

3. a. Comparison of the experimental stress-strain curve of specimens 9 to the numerically obtained stress strain curves. b. Same as (a) for specimen 5. c. The experimental measured velocities of specimens 7-11 and their digitized approximation d. Same as (c) for specimens 4-6.

Fig. 11 Numerical map contours at $\hat{\varepsilon}_{zz} = 0.2$. The maps correspond to specimens 4-6 of table 3. The assumptions: $f = 0.3$ and $\beta = 15^{\circ}$ are used and the applied velocities of Fig. 10(c). The horizontal line is the deformed "mid-height line" seen in Fig. 8(a). a. True strain (ε_{zz}) b. True stress (σ_{zz}). c. Radial stress (σ_{rr}) . d. Shear stress (σ_{rz}).

Fig. 12 The applied external work and the dissipated frictional work and the ratio between them as a function of the true strain during an experiment in a SPHB. The curves represent the behavior of specimens 4-6 of table 3.

Fig. 13 Effect of β on the averaged values on the mid-height line. a. confinement pressure. b hydrostatic pressure. c. equivalent Mises stress.

FIGURES

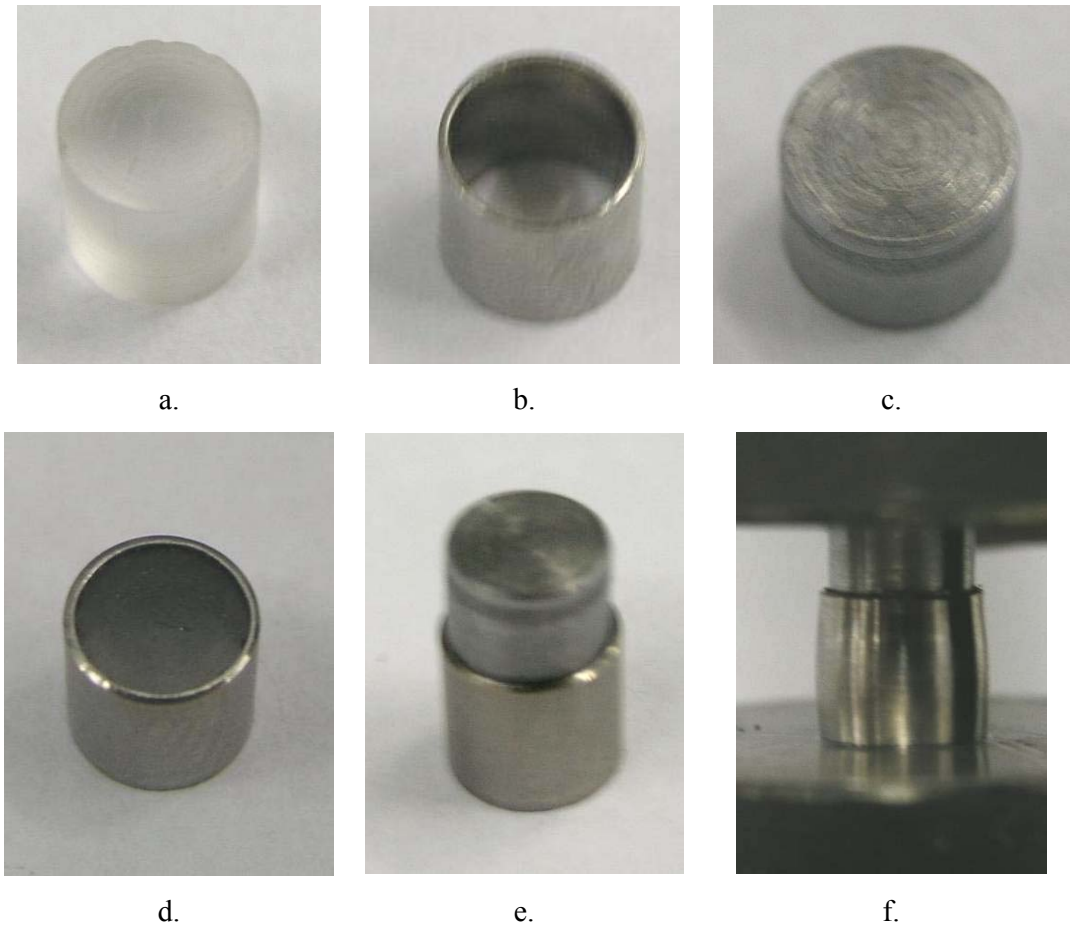

Fig. 1. The specimen assembly. a. Cylindrical polycarbonate specimen. b. Metallic sleeve. c. Adapter which is used to apply pressure to (a). d. Assembly of the specimen into the sleeve. e. Assembly of the adapter (c) on top of the confined specimen. f. The assembled specimen under quasi-static compression testing.

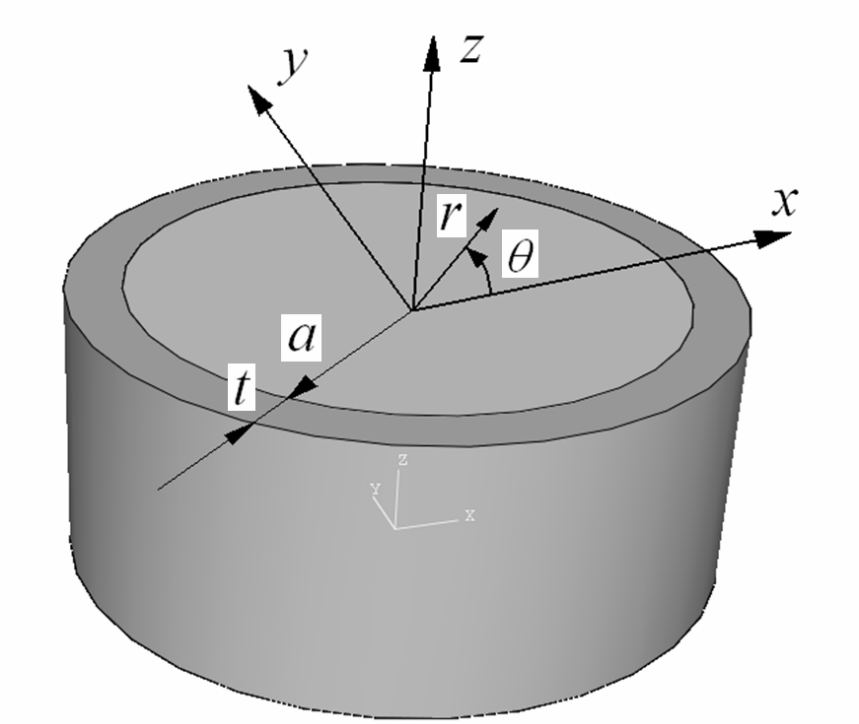

Fig. 2. A cylinder with an outer radius a and a sleeve of thickness t with cartesian and cylindrical coordinate systems attached to it.

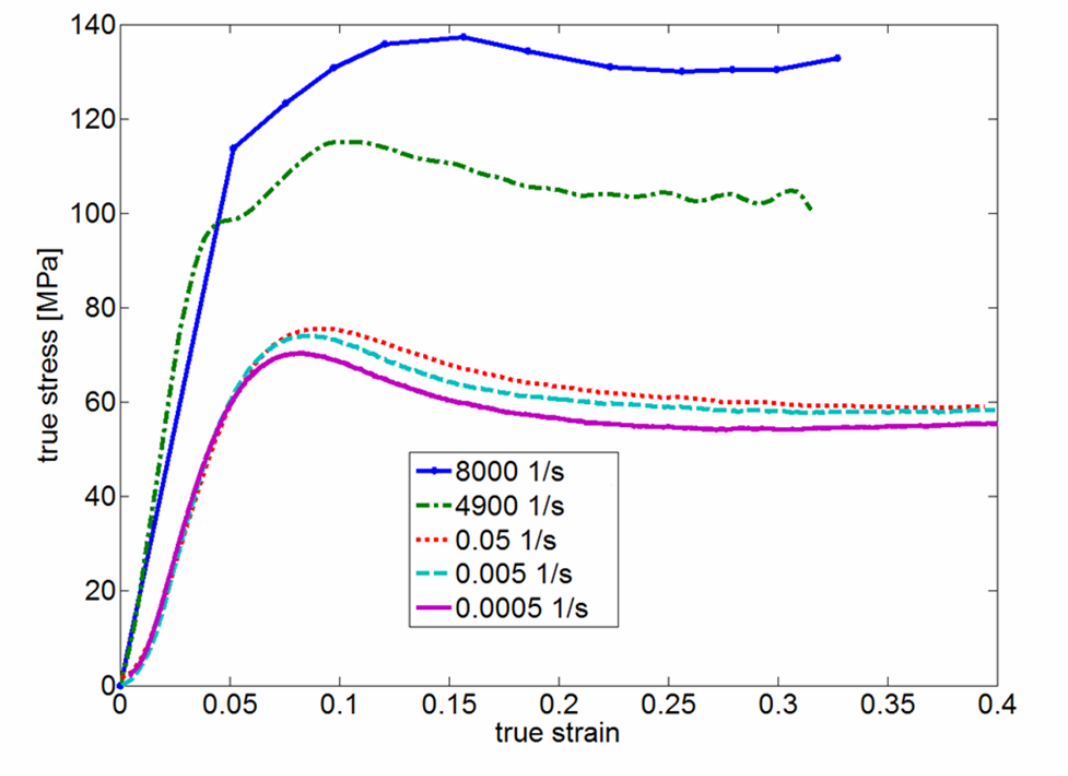

Fig. 3. True stress–strain curves for unconfined specimens (1-3) along with typical dynamic results. The high strain-rate sensitivity of PC is noticeable.

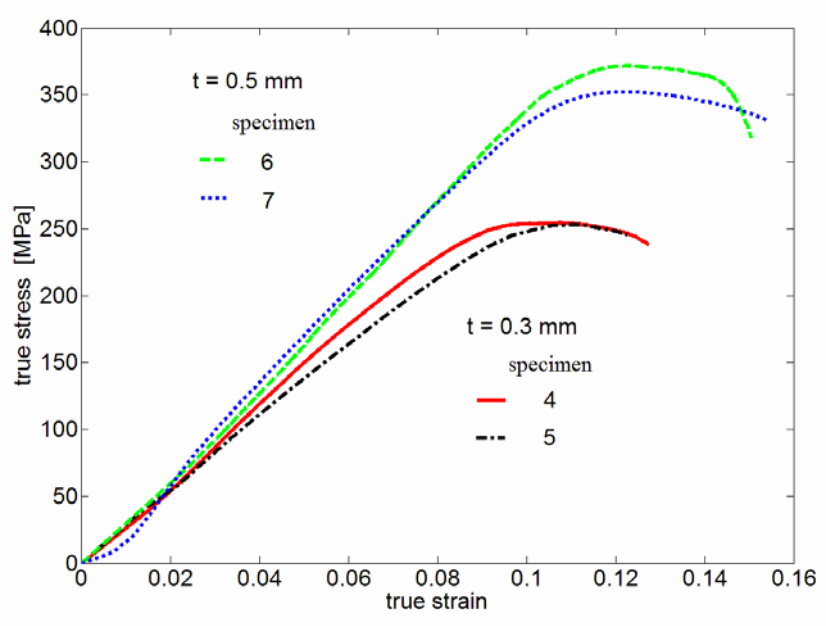

a

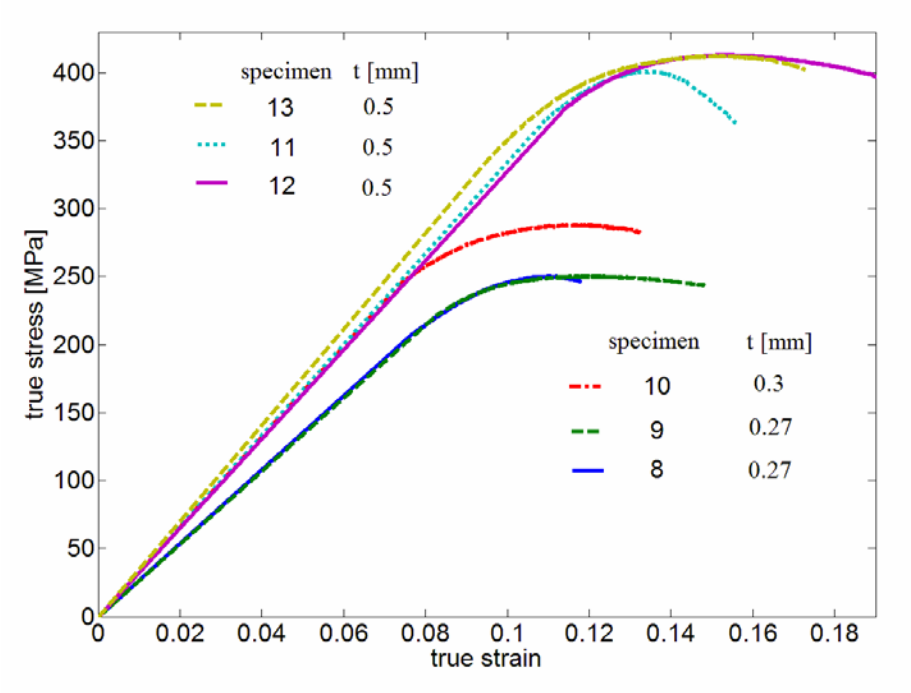

b

Fig. 4. Quasi static experimental results of confined specimens. a. Specimens 4-7 of table 2 confined with sleeve made of M 250 steel . b. Specimens 8-13 of table 2 confined with sleeves made of M 300 steel.

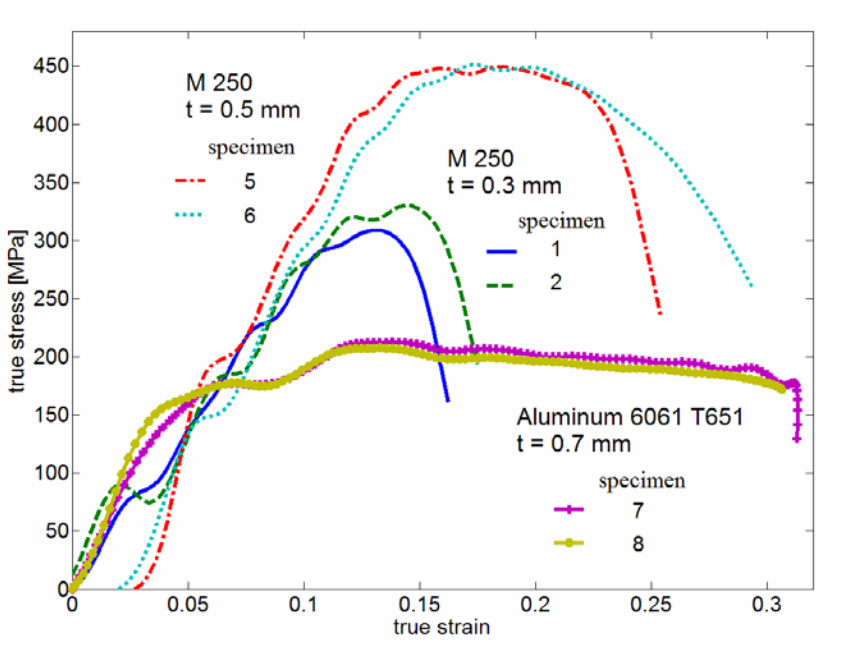

a

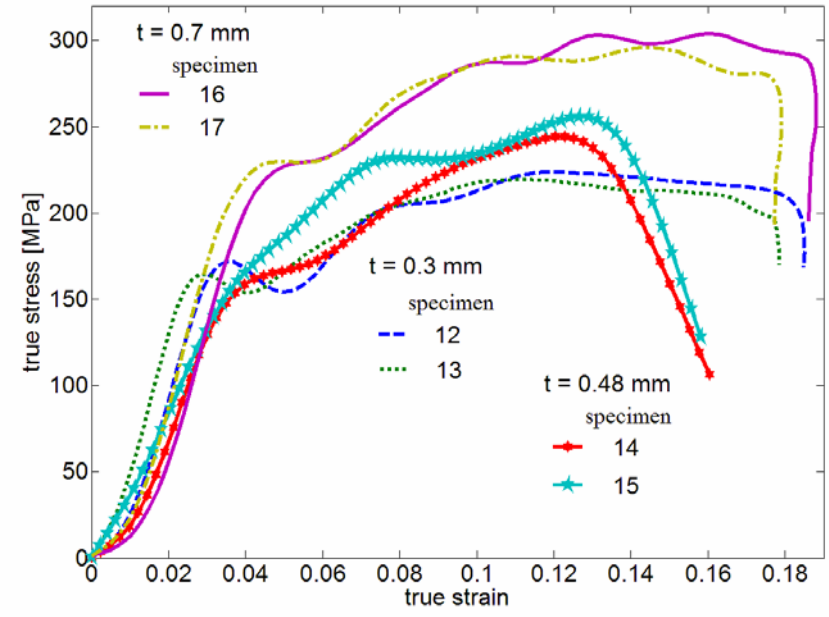

b

Fig. 5. Dynamic experimental results . a. Specimens 1, 2, 5 and 6 of table 3 confined with M 250 sleeves, and specimens 7-8 of table 3 confined with aluminum 6061 sleeves. b Specimens 12-17 of table 3 confined with 1020 steel sleeves.

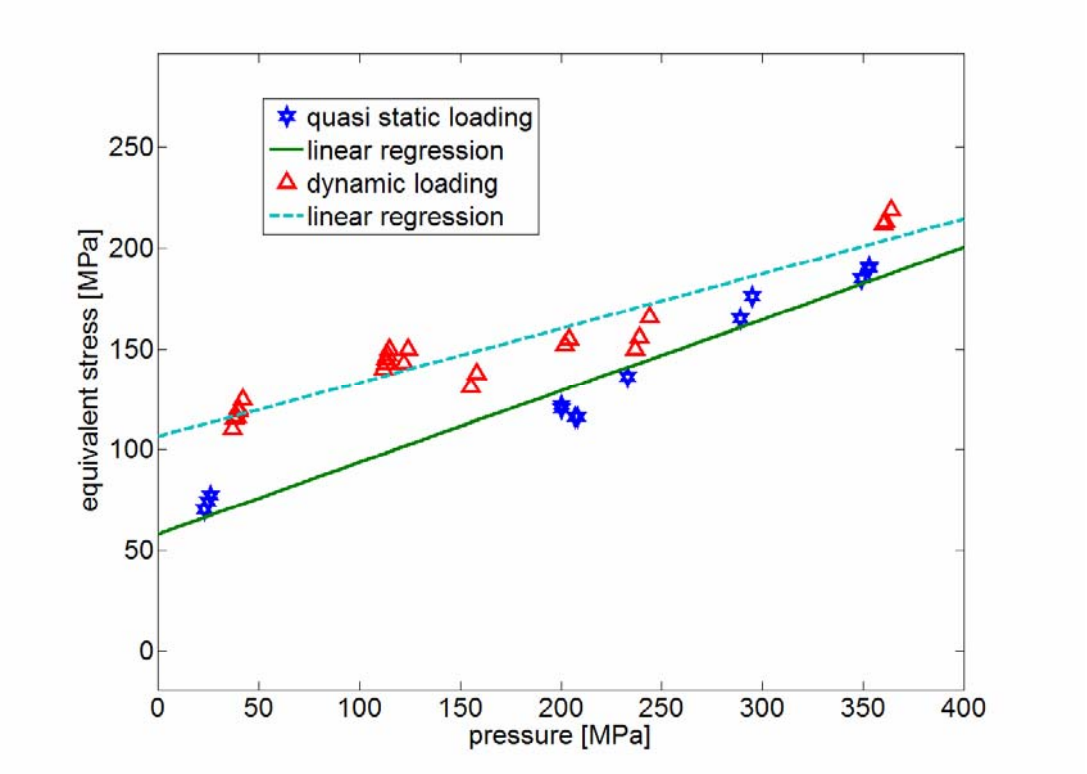

Fig. 6. Quasi static and dynamic experimental results of the equivalent stress vs. pressure.

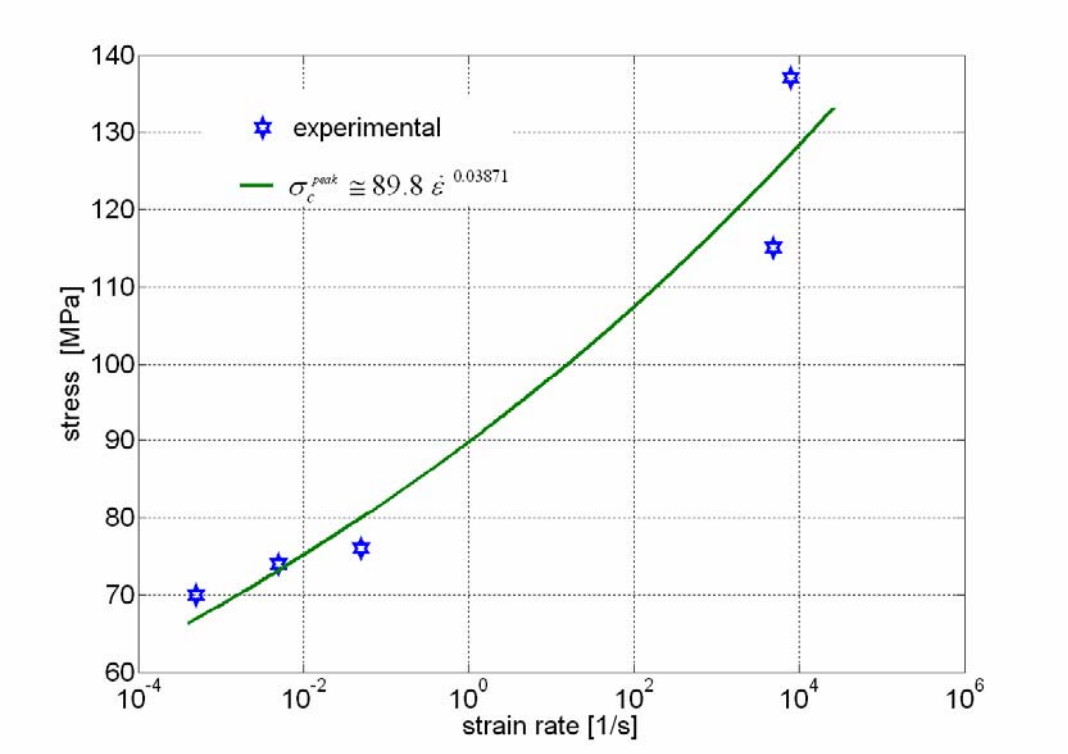

Fig. 7. Strain rate sensitivity of unconfined polycarbonate. The stress is measured at its peak value.

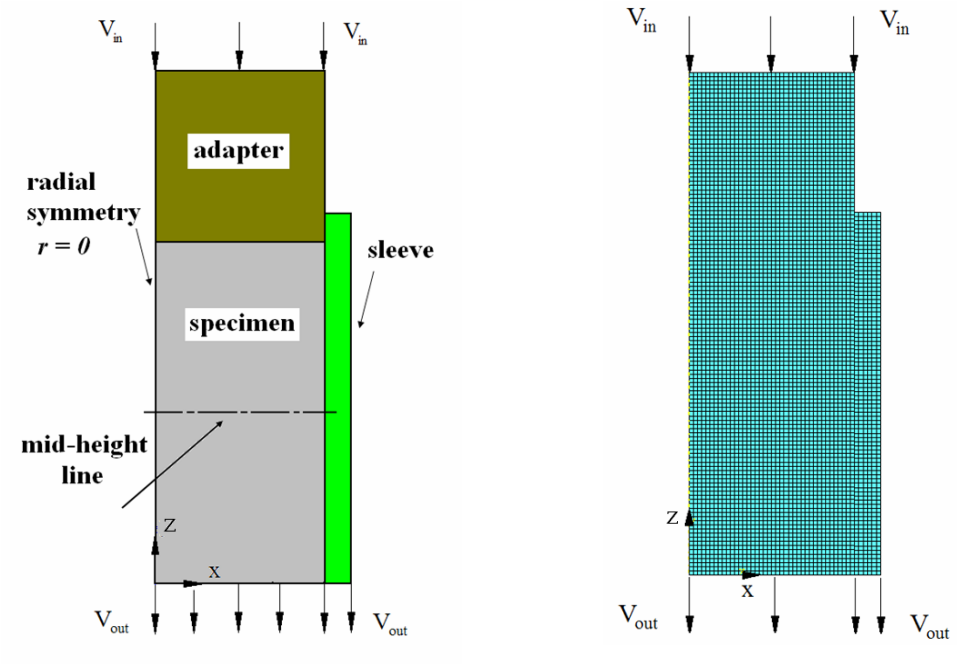

a. b.

Fig. 8. The axisymmetric assembly model with a coordinate system and arrows indicating the location of the applied velocities in the dynamic simulations. a. The geometrical model which consists of three parts: specimen, sleeve and adapter. b. A typical meshed model with quadrilateral elements.

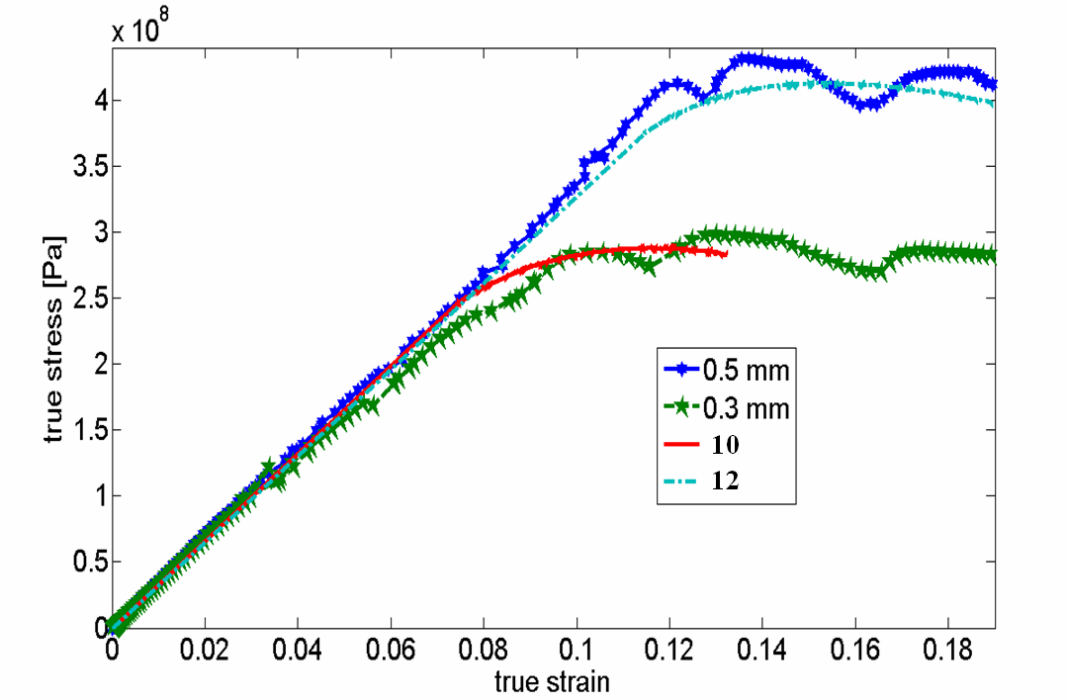

Fig. 9. Comparison of the experimental stress-strain curve of specimens 10 and 12 of table 2 to the numerical stress strain obtained by solving quasi- statically with the assumption of $f = 0.3$ and $\beta = 15^{\circ}$. Note the very good agreement between the experiments and the simulations for this set of parameters.

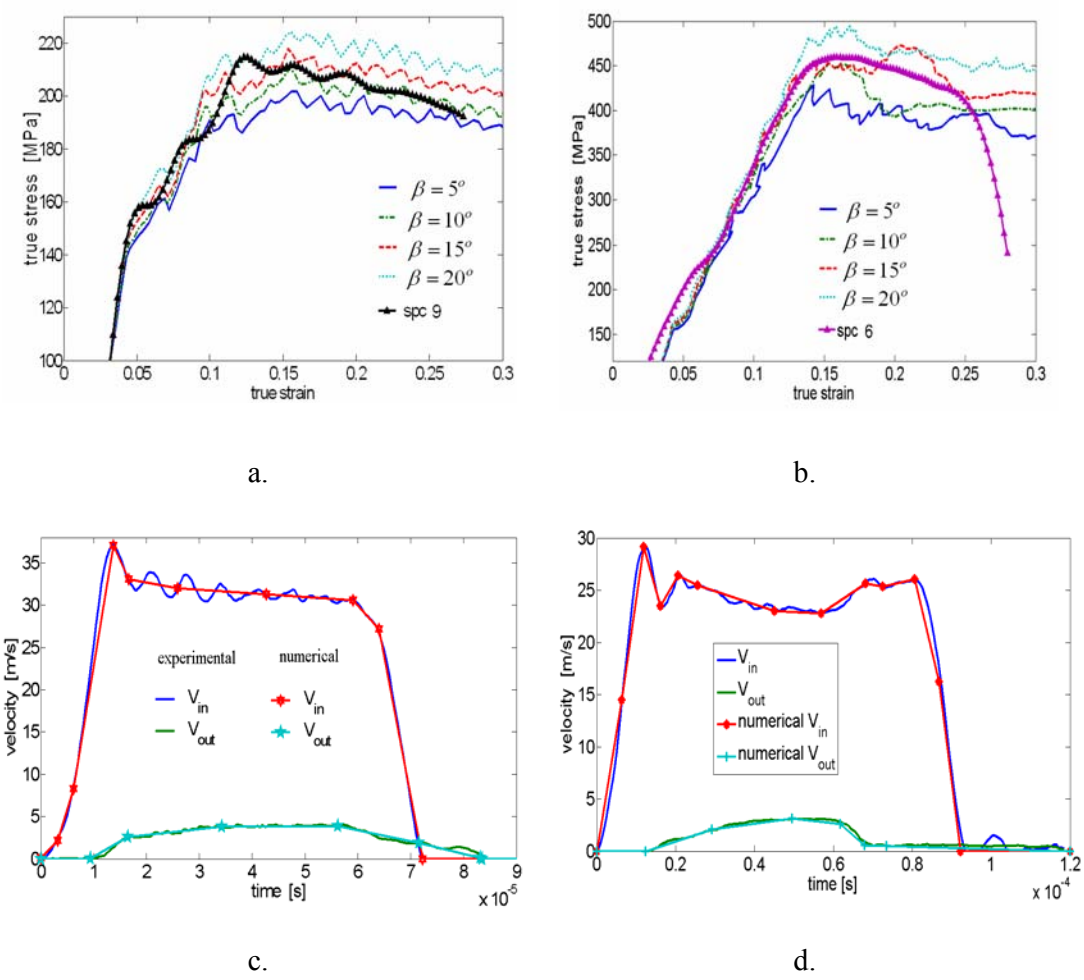

Fig. 10. Numerically calculated stress strain curves for $f = 0.3$ and $\beta = 5^\circ, 10^\circ, 15^\circ$ and 20°, and experimental results together with their corresponding typical applied velocities. The specimens are detailed in table 3. a. Comparison of the experimental stress-strain curve of specimens 9 to the numerically obtained stress strain curves. b. Same as (a) for specimen 5. c. The experimental measured velocities of specimens 7-11 and their digitized approximation d. Same as (c) for specimens 4-6.

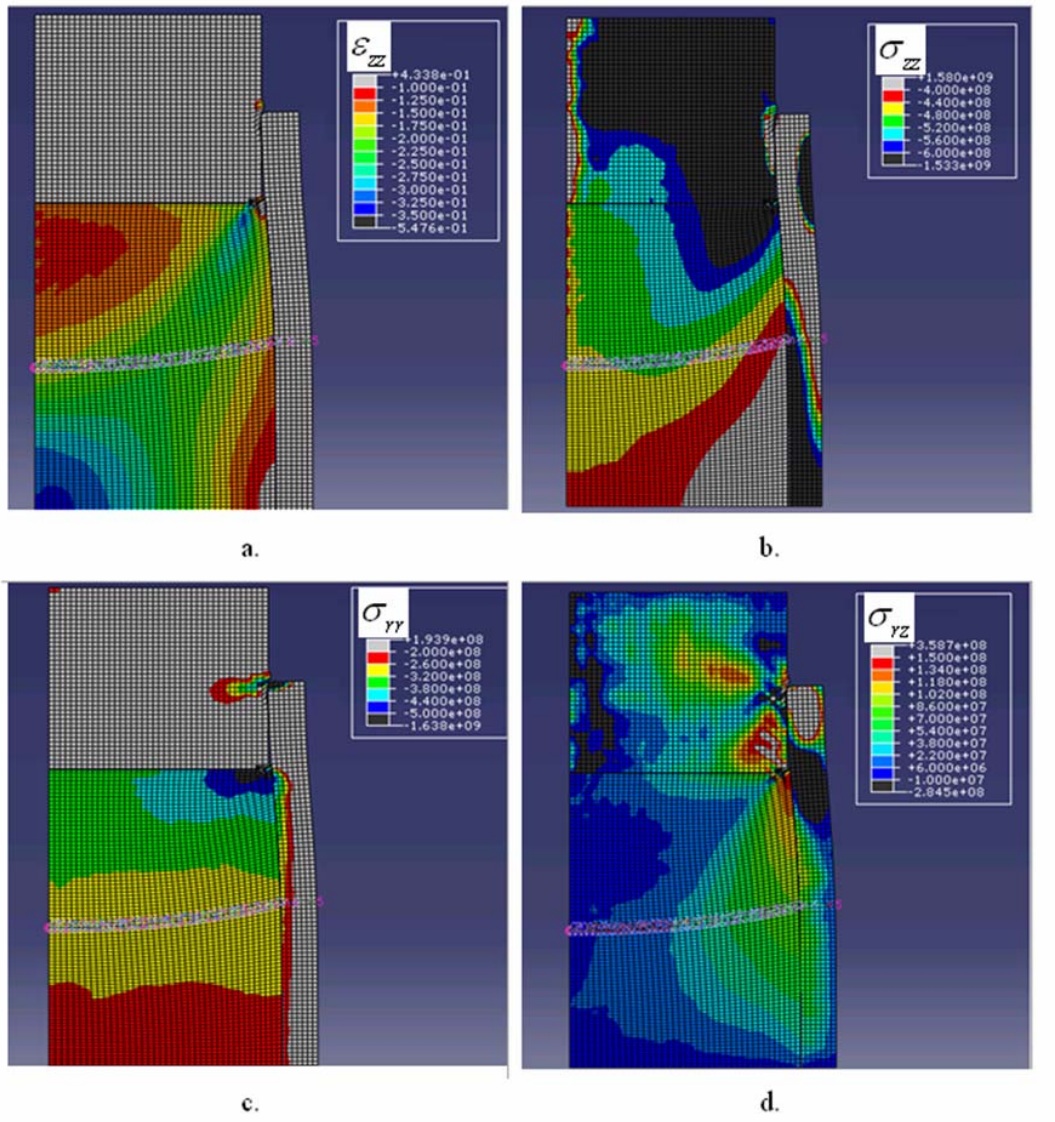

Fig. 11. Numerical map contours at $\hat{\varepsilon}_{zz} = 0.2$. The maps correspond to specimens 4-6 of table 3. The assumptions: $f = 0.3$ and $\beta = 15^{\circ}$ are used and the applied velocities of Fig. 10(c). The horizontal line is the deformed "mid-height line" seen in Fig. 8(a). a. True strain (ε_{zz}) b. True stress (σ_{zz}). c. Radial stress (σ_{rr}) . d. Shear stress (σ_{rz}).

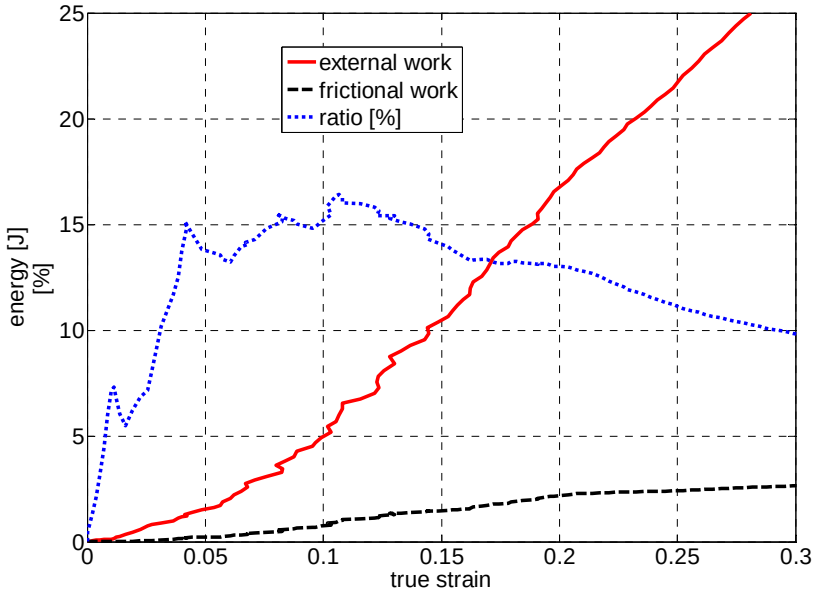

Fig. 12. The applied external work and the dissipated frictional work and the ratio between them as a function of the true strain during an experiment in a SPHB. The curves represent the behavior of specimens 4-6 of table 3.

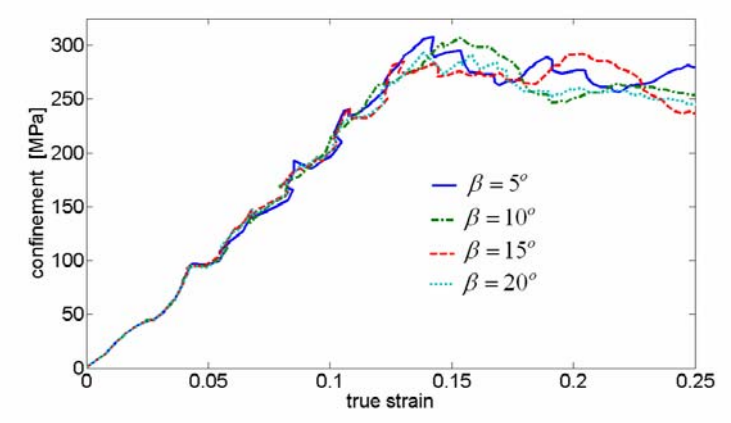

a.

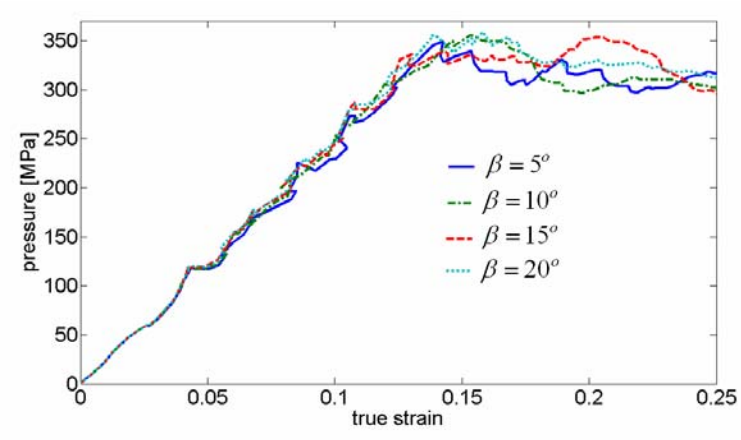

b.

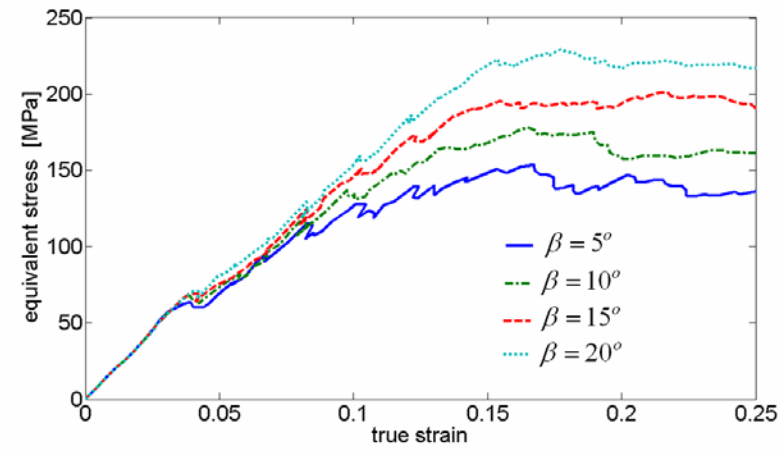

c.

Fig. 13. Effect of β on the averaged values on the mid-height line. a. confinement pressure. b hydrostatic pressure. c. equivalent Mises stress.